

Raman spectroscopy of active-carbon electrodes when Au colloids are placed at the electrolyte/electrode interface

H. Grebel⁽¹⁾ and Yuanwei Zhang⁽²⁾

⁽¹⁾ Center for Energy Efficiency, Resilience and Innovation (CEERI) and the ECE Department at the New Jersey Institute of Technology, Newark, NJ 07102. grebel@njit.edu

⁽²⁾ Department of Chemistry and Environmental Science at the New Jersey Institute of Technology, Newark, NJ 07102. yuanwei.zhang@njit.edu

Abstract:

In the past, when Au nanoparticles (AuNPs) were placed just above (but not included in) active carbon (A-C) electrodes, a 10-fold amplification of gravitational specific capacitance were demonstrated, despite the small mass-ratio between the AuNPs and A-C; a ratio of 1:5000. We use surface enhance Raman spectroscopy (SERS) in further studying this system. Supercapacitors are volumetric elements while SERS is a surface interrogating method, whose signal could be impacted by many factors, including local colloid's preferential points (hot spots). Here, we use the ratio between the D- and G-lines of the A-C electrode, I_D/I_G , as a marker to eliminate the surface inconsistencies. At some concentration levels of AuNPs, the A-C Raman signature shows a clear preference towards the 1600 cm^{-1} vibration mode (G-line). Following that point, the cell exhibits a large specific capacitance.

I. Introduction

Super-capacitors (S-C) take advantage of the large capacitance at the narrow interface between a porous electrode and an electrolyte. Here we concentrate on carbon-based S-C that exhibit electrical double-layer [1-4]. Supercapacitors are used in a wide-range of applications, such as consumer electronic products, memory back-up devices, hybrid electric vehicles, power supply system [5,6]. They were also proposed as buffers to highly fluctuating power grids that are equipped with sustainable sources [7]. Thus, increasing the capacitance of existing super-capacitors may prove useful for these application.

Our structure is rather simple: in addition to a typical cell, composed of electrolyte, active-carbon and current-collector we have added very low dispersion of gold colloids (AuNPs) to the mix [8]. The AuNPs are held by electrostatic forces: between a ligand that coats them and the A-C electrodes and proved to be very strong upon washing. One ought to note that the Au colloids are not placed within the A-C particulate, but rather on its surface at a short distance from it. Placing the AuNPs inside the A-C particulate would result only in an impedance change of the electrode itself with little effect on the cell capacitance.

Incorporating metal features into dielectrics increases ordinary cell's polarization [9-13] - a field known as Artificial Dielectrics (AD). This is true in the quasi-dc regime where a 10-fold enhancement in the specific capacitance of A-C electrodes was shown [8] despite the large mass difference between the AuNPs (of the order of tenths of micro-grams) and the A-C (of the order of 100 to 200 mg). This polarization effect is also true for the visible and IR region - metal colloids exhibit Raman enhancement (Surface Enhanced Raman Spectroscopy, SERS [14-18]) and IR signals enhancement (Surface Enhanced IR Absorption, SEIRA, [19,20]). Therefore, it would be natural to combine SERS in the study of metal colloids and super-capacitors, similarly to ordinary Raman [21,22].

Dispersions of the Au nano-particles (AuNPs) have been known for a long time. Their preparation methods are well-established, as well as, the relationship between their size, as determined by SEM or TEM and their optical scattering properties [23,24]. In order to ensure a good suspension, the colloids are functionalized with a negatively charged ligand. While the plasmonic peak absorption of uncoated AuNPs dramatically changes as a function of particles size [25], it is much less so for ligand coated particles [26]. A well-established technique that correlates the particle size to its optical scattering is dynamic light scattering (DLS) [27], which is used to determine the average particle size. The electrode itself is charge-neutral. Nevertheless, there is an electrostatic bond between the neutral, yet conductive A-C electrode and the negatively functionalized AuNPs. We use this bond to attach the AuNPs to the A-C electrode.

In general, for SERS under dry condition the larger the particle is the better [28,29]. For super-capacitors, the capacitance effect takes place within the thin interface between the electrolyte and a solid electrode. Thus, the effectiveness of smaller particle that fit into the interface could make a relatively larger impact unlike the larger ones. Using a full wave analysis, the closer is the colloids to the electrode, the larger is the supercapacitive effect [30,31], similar to SERS.

In this paper we set to investigate the use of SERS in AuNPs imbedded supercapacitors where the gold colloids are separated from the A-C electrodes by a small ligand.

II. Materials and Methods

II.a Preparation methods - gold colloids:

In-house, AuNPs were synthesized by following a well-established method [27]; it employs citrate as a reducing agent and stabilizer. In brief, chloroauric acid (HAuCl_4) water solution (10 mg HAuCl_4 in 90 mL of water) was heated to boiling and sodium citrate solution (0.5 mL of 250 mM)

was introduced. The mixture was stirred for 30 min until the color turned to wine red, or purple-brown. AuNPs were then purified by centrifuge and washed with DI water three times. The concentration of AuNPs in water was 1 mg/mL; the titration experiments were made with increasing amounts of 10 μ L per batch and are translated to μ g when referenced to the amount of A-C in the batch. The other batches were purchased from a vendor (Fisher), their concentration was much less. There were several batches of suspended AuNPs that have been used: commercial 40 and 100 nm (Thermo Fisher Chemicals, supplied in 0.1 mg/mL sodium citrate with stabilizer) and home-made (45 nm, [8], coated with sodium citrate). The Zeta potentials for the coated AuNPs were, -31.1 mV and -17.8 mV for the 45 nm and 40 nm, respectively. The Zeta potentials for the coated AuNPs were, -31.1 mV, -17.8 mV and -23.2 mV for the 45 nm, 40 nm (as is) and 100 nm (as is) and -33.6 mV for a concentrated batch of 40 nm colloids.

II.b. Preparation methods - the porous electrodes:

A 100 mg of Cellulose Acetate Butyrate binder (CAB, Aldrich Chemicals) were first dissolved in 20 mL of acetone. 2 g of active-carbon (A-C, specific surface area of 1100 m^2/g , produced by General Carbon Company, GCC, Paterson, NJ, USA) were added and sonicated for 1 hour using a horn antenna. Vials, each containing 2 mL of the slurry were prepared. To these, succession amounts of 10 μ L of AuNPs, suspended in water were added. Each mixture was further sonicated with the horn antenna for additional 30 min. The slurry was dropped casted on grafoil electrodes (area of contact 1.27x1.27 cm^2 , manufactured by Miseal and purchased through Amazon), baked on a hot plate at <90 °C and then soaked with an electrolyte (1 M of Na_2SO_4 , $NaCl$, or KOH). A fiberglass filter (Whatmen 1851-055), or a paper filter were used as a membranes. The Au colloid concentration were respectively, 1 mg/mL (home-made) and 0.1 mg/mL (Fisher). The Au colloids sizes were of order of ~40 and 100 nm (Fisher), 45 nm (home-made). For the 40 and 100 nm colloids we used poly vinyl alcohol (PVA) as a binder (instead of the CAB). The PVA was dissolved in disulfide methyl sulfoxide (DMSO). Due to the lower concentration of the colloids, we added DMSO to the titration vials in order compensate for the added colloids volume in the sample.

On the average, the A-C particulates' dimension were ca 15 microns [29-30] and their specific surface area was rated as 1100 m^2/g .

II.c. The samples:

Cuts of 200 micron thick grafoil electrodes with back adhesive (1.27 cm x 2.54 cm) were placed on similar cut microscope slides. Before placing it on the slides, the grafoil electrodes were heated for a few hours. The two slides were held by tweezers (or plastic clips) and the boundaries of the sample were left unsealed while soaking it in the electrolyte. The samples were later sealed with an epoxy. A hole was cut through the upper electrode for the Raman laser beam. The sample configuration is shown in Fig. 2a and its picture in Fig.2b.



Figure 2. (a) A cross section of sample with grafoil coated active-carbon (A-C) electrodes, and (b) a picture of the sealed sample, covering area of ca. $1.27 \times 1.27 \text{ cm}^2$ with an entrance hole. The number on the right indicates sample zero.

II.d. Electrochemical Techniques:

Potentiostat/Galvanostat (Metrohm) was used in a 2-electrode set-up. Most data here is provided with Cyclic Voltammetry (C-V) at scan rates of 100 mV/s. Charge-Discharge (C-D) at applied currents of 1 and Electrochemical Impedance Spectroscopy (EIS) between 50 kHz to 50 mHz completed the test. The results all agreed on the titration trends.

II.e. Raman Measurements:

The Raman system was made of 75-cm spectrometer equipped with a camera (cooled to 50 °C). A coherent laser, at $\lambda=532 \text{ nm}$, with intensity of $I=5 \text{ MW}$ at the sample and $\times 10$ objective were used. After averaging, the data was fit with two Lorentzians. In Figure 3 we show a typical Raman spectra of the A-C and its current collector (grafoil). The A-C exhibit two peaks in the range of 1200-1800: one at 1314 (the D-line) and the other at 1582 cm^{-1} (the G-line). The grafoil has a single G-line peak at 1570 cm^{-1} .

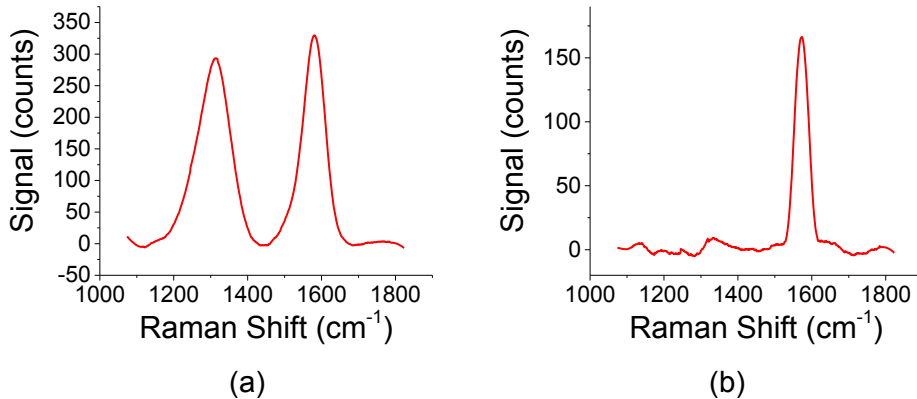


Figure 3. Smoothed Raman spectra of dry A-C and (b) of the grafoil current collector

II.f. Initial Characterizations:

While measurement on supercapacitors are made on a bulk sample, thus averaging any local effect, Raman measurement are quite local and could be affected by the number of local colloids and their separation. Figure 4a shows two Raman signals for 100 nm sample: one at some 'random' position, and the other for a 'preferred' position where the signal was maximized. Both signals were taken under dry conditions. The curves conveys two points: (a) the ratio I_D/I_G is fairly

constant regardless of the measurement conditions and (b) there is characteristic dip in the curve, which suggests a preferred Raman excitation. We will try to correlate the I_D/I_G ratio with the gravitonic specific capacitance.

In order to make all sample roughly measured under similar conditions, we use 100 μL of the 0.1 mg/mL batch for each titration sample (thus, 100 μL of this sample per 200 mL of A-C). The inclusion of ionic environment makes the situation most complex. That is shown in Fig. 4b when the peak of 70 $\mu\text{g}/200$ mg of A-C of Fig. 4a has shifted to 50 $\mu\text{g}/200$ mg of A-C. The gravitonic specific capacitance of this relatively diluted 100 nm colloids (Fig. 4c) does not convey a clear peak within this measurement range, as we shall see below. Conditions: C-V at 100 V/s; PVA binder; electrolyte - Na_2SO_4 ; glassy separator.

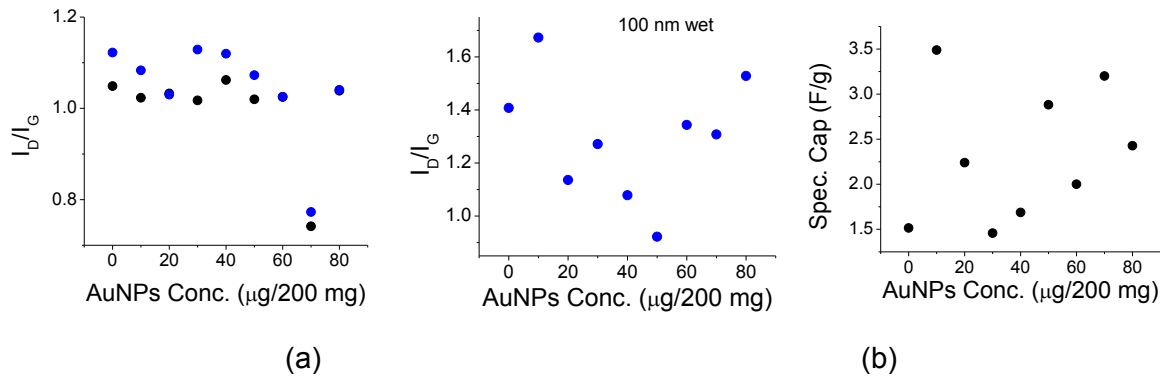


Figure 4. 100 nm sample. (a) The ratio of I_D/I_G for dry. Blue - preferred measurement position; Black - random measurement position. (b) I_D/I_G ratio for wet samples. (c) The gravitonic specific capacitance. The sample concentration was rated as 0.1 mg/mL of ligand weight. Successions of 100 mL per titration was used per 200 mg of A-C.

III. Results

III.a. As-is 40 nm colloid:

40 nm colloidal AuNPs in PVA bound, A-C cell are shown in Fig. 5. The sample is rated by the manufacturer as 0.1 $\mu\text{g}/\text{mL}$ of the ligand weight (which typically means several ligand layers). In order to make all sample roughly measured under similar conditions, we use 100 μL for each titration sample (thus, 100 μL per 200 mL of A-C in our original). The peak of 70 $\mu\text{g}/200$ mg of A-C of Fig. 4a has shifted to 30 $\mu\text{g}/200$ mg of A-C (Fig. 5a). The specific capacitance shows a clear transition at 30-40 $\mu\text{g}/200$ mg per 200 A-C. Conditions: C-V at 100 V/s; PVA binder; electrolyte - Na_2SO_4 ; glassy separator.

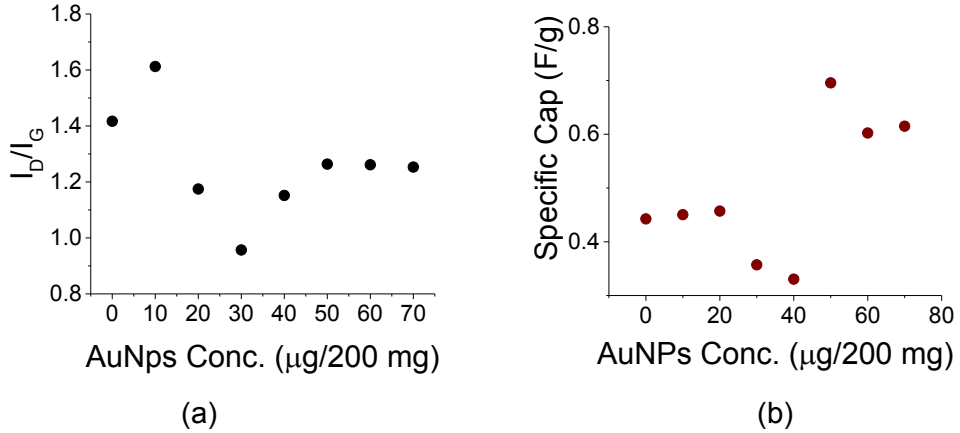


Figure 5. As is, un-concentrated 40 nm sample. (a) The ratio of I_D/I_G for a dry sample and (b) the gravitonic specific capacitance

III.b. 40 nm colloid - concentrated:

In order to reduce the amount of water, present in the low original 0.1 mg/mL AuNPs batch concentration, we evaporated it reach a concentration of 0.5 mg/mL. In this case we used 20 μg/mL per titration (or 20 μg/mL per titration per 200 mg of A-C). Under wet conditions, Fig. 6a a minima in the I_D/I_G for wet conditions at 10 μg/200 mg of A-C. Fig. 6b exhibit a clear maxima in the specific capacitance at 30 mg/200 mg of A-C. Conditions: C-V at 100 V/s; PVA binder; electrolyte - NaCl, separator - paper filter).

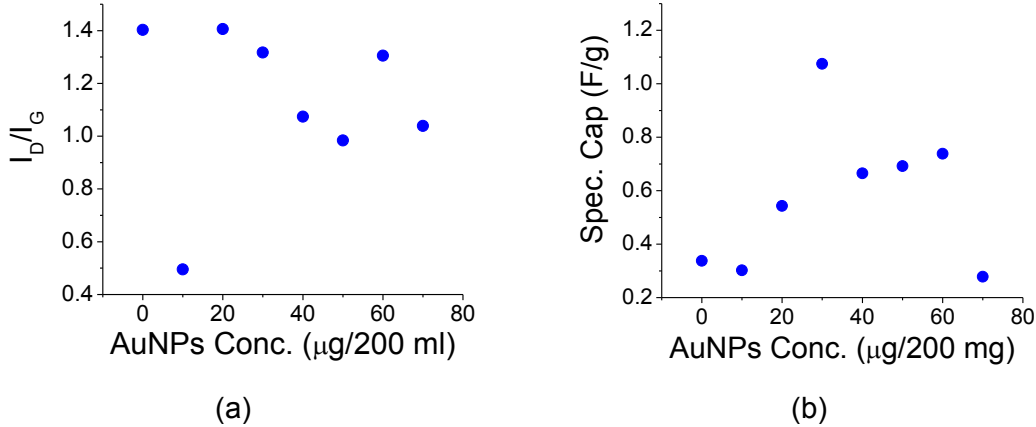


Figure 6. Concentrated 40 nm sample. (a) The ratio of wet I_D/I_G . (b) The gravitonic specific capacitance.

III.c. 45 nm colloid:

It seems that thin ligands are better in terms of influence on the batch integrity and clarity of signals. Our home-made, single-layer sample In Figs. 7-8. The concentration of the AuNPs was 1 mg/mL. As in [8], we use 10 μg per titration per 200 mg of A-C. The dry 45 nm sample exhibited a minima at $I_D/I_G=30$ μg/200 mg of A-C (Fig. 7a), whereas the wet sample exhibited a minima at a lower value, around $I_D/I_G=10$ μg/200 mg of A-C (Fig. 7b). Condition: (C-V at 100 V/s; PVA binder; electrolyte - Na_2SO_4 ; glassy separator).

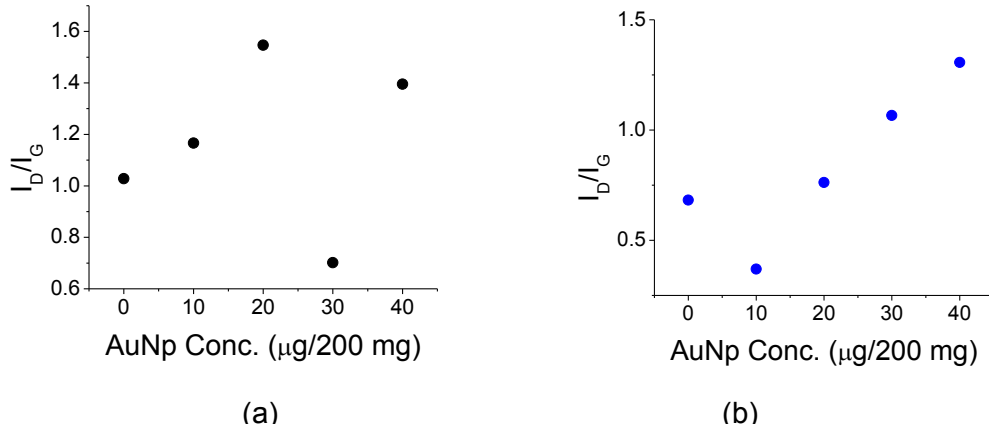


Figure 7. 45 nm sample. (a) The ratio of I_D/I_G under dry and (b) under wet conditions.

The gravimetric specific capacitance exhibit a peak at 30 $\mu\text{g}/200 \text{ mg}$ (Fig. 8a) and the A-C, G-line exhibits a large value at the same point (Fig. 8b). The later implies that the D-line of the A-C was large, as well. The, D-line exhibits a slight shift as a function of bias (Fig. 8c).

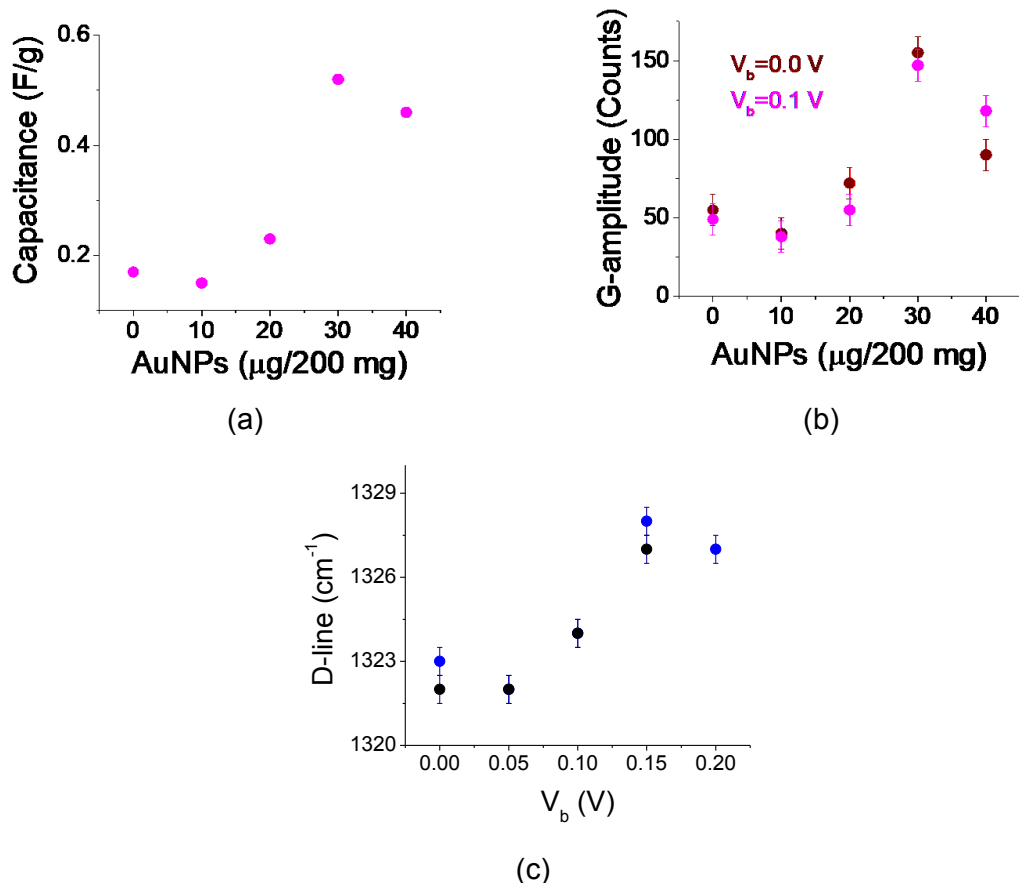


Figure 8. 45 nm sample. (a) Gravitonic specific capacitance as a function of titration. (b) The A-C G-line as a function of bias under wet conditions. (c) Change in the D-line of A-C as a function of bias: black curve - in the up direction; blue curve - in the down direction.

IV. Discussion

At first glance, there should be no connection between the high-frequency surface enhance Raman scattering (SERS) and the low frequency of super-capacitors. One is a local surface technique and the other is an averaged, volumetric system. The connection is more apparent if one may find a marker that eliminates the surface imperfections. One should note that the gold colloids are coated with a ligand that keeps them from coagulating, so the discussion should be limited up to its critical concentration point.

Under dry and wet conditions, SERS exhibited a large change in the I_D/I_G ratio, which showed a preference toward the G-line at some AuNPs concentration. The I_D/I_G ratio of wet samples was shifted with respect to dry samples. This indicates the effect of the ions in the electrolyte [22]. The supercapacitor cell also showed a large specific capacitance at similar AuNPs concentration levels. The specific capacitance is a convenient parameter across samples with varying thicknesses.

The D-line of A-C is the result of interaction between the laser radiation and the charges that surrounds a defect point [32-33]. The G-line are the interaction of basal vibrations between typically, a few graphitic lines. Since in general, the D- and G-lines are independent of each other, it is surprising to find a concentration value for the AuNPs that is enhancing one line over the other.

Local field models: We use a static model (Lorentz model) to better understand the connection between SERS and AuNPs-embedded S-C. As the concentration of AuNPs increases, so is the effect of neighboring colloids. Namely, the local field at some particular colloid position is a linear combination of the external field (the laser light, or the external cell bias) and an interaction field from all other neighboring colloids. The effect of all other colloids is characterized by an interaction parameter, C, which can be assessed by the potential of all other colloids on the colloid of interest (excluding the colloid itself). For a two dimensional case (one layer of colloid on the cell's electrode) the effect is proportional to the average distance between the colloids to the third power.

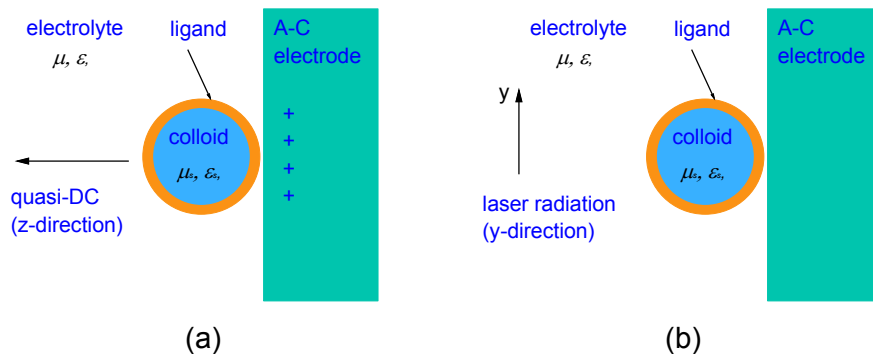


Figure 9. (a) Quasi-DC model. (b) SERS model.

Low frequency model: At very low frequencies, the interaction field is mostly of electric nature. The induced polarization on a spherical object is written as, $p = \epsilon_0 \alpha_e E_0$, with ϵ_0 - the vacuum dielectric constant; α_e - the colloid polarizability and E_0 is the external field between electrodes. The local polarization is achieved in a self-consistent form, the Clausius-Mossotti relation and noting that the macroscopic polarization is $P=Np$ [10]. This is true when the distance between

colloids is much smaller than the wavelength of interest and easily achievable at low frequencies of cell's operation [10]:

$$P = N\epsilon_0\alpha_e E_0 / (1 - \alpha_e C). \quad (1)$$

Along the z-direction (the direction perpendicular to the cell electrodes, Fig. 9a), the coupling constant, C_{LF} , may be derived for two dimensional array of colloids, $C_{LF} = -2.4/\pi a^3 + (16\pi/a^3)K_0(2\pi)$, with the average distance between colloids is "a", and K_0 is the modified Bessel function, $K_0(2\pi) = 0.001$. For metals, the metal polarizability is $\alpha_e = 4\pi r_0^3$, with r_0 being the colloid radius. The negative coupling constant, $C_{LF} \sim -2.4/\pi a^3$ implies that the colloid is highly polarizable, opposing the external field. When the colloid of a fixed radius r_0 fills the interface between the liquid and A-C electrode (including the diffusion layer), the density of colloids is, $N \sim a^2 \cdot r_0$. The effective dielectric constant with respect to the electrolyte background (without the colloids) is $k = 1 + N\epsilon_0\alpha_e E_0 / (1 - \alpha_e C) = 1 + 4\pi r_0^3 / r_0 a^2 / (1 + (2.4/\pi) \cdot 4\pi r_0^3 / a^3)$. The effective dielectric constant is directly related to the capacitance increase in supercapacitors and is plotted in Fig. 10. The model predicts an increase of ~ 2 in the capacitance, lower than is typically measured. It is limited by $2r_0/a \sim 1$ and perhaps long before that (see Fig. 4a vs Fig. 6b or, 8a). Beyond that point, the ligand prevents formation of a colloidal array and becomes erratic. In general, the model predict a 20% dielectric change and a larger concentration range when the AuNPs are changed from 40 nm to 100 nm. Full wave simulations indicate that the large polarization spots are directly under the colloids, between the colloid and the A-C electrode [8].

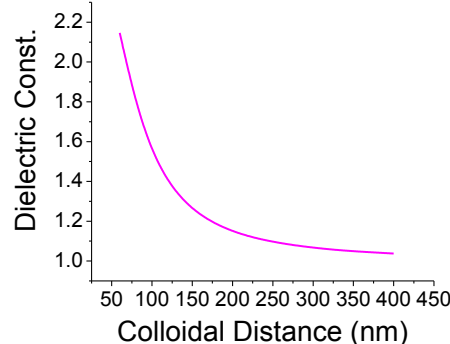


Figure 10. The relative change in the dielectric constant as a function of particle distance in nm for a 45 nm colloids. The titration is typically conducted from large to smaller distances.

High-frequency model: We treat it as a propagation problem. The A-C molecules is at close proximity to the colloids and are interrogated by a high-frequency laser beam. The field is transverse to the electrode surface (Fig. 9b, s-polarization). SERS has two enhancement factors: one from a single colloids and the other through the local field enhancement of the other colloids. We have a monolayer of colloids at the electrode's surface, and the magnetic field is much smaller than the electric one at the near-field.

The *molecular* polarizability, α_m is expanded (one dimension) as, $\alpha_m = \alpha_{m0} + (\partial\alpha_m/\partial x)_0(\delta x)$ to account for the (linear) molecular vibrations, δx . The interaction between the vibrating molecule (the A-C electrode) and the laser radiation, E_0 , is written as: $p_{\text{Raman}} = \epsilon_0 \cdot (\partial\alpha_m/\partial x)_0 \cdot (\delta x) \cdot E_0$. The vibration mode, (δx) , may be solved by use of induced harmonic oscillator, $(\delta x) = \epsilon_0 \cdot (\partial\alpha_m/\partial x)_0 \cdot E_0 \cdot E_{\text{Raman}}$. In the presence of a single gold colloid, the NL polarization is enhance by a gain coefficient, $g \sim (r_{\text{colloids}})^4$, with r_{colloids} being the colloid's radius [28].

The effect of many colloids on SERS may be added to each of the participating field component, incident and Raman components, through a polarization term, $E_0^{\text{local}} = E_0 + \alpha_e C_{\text{HF}} / \epsilon_0$, and $E_{\text{Raman}}^{\text{local}} = E_{\text{Raman}} + \alpha_e C_{\text{HF}} / \epsilon_0$, respectively. Note the polarizability, α_e , is of the colloids, not the molecules. The entire polarization with is:

$$p = (p_{\text{clear}} + p_{\text{SERS}}) = \epsilon_0 \alpha_e (E_0^{\text{local}} + E_{\text{Raman}}^{\text{local}}) + g \cdot (\epsilon_0)^2 \cdot (\partial \alpha_m / \partial x)^2 \cdot (E_0^{\text{local}})^2 \cdot (E_{\text{Raman}}^{\text{local}}). \quad (2)$$

Frequency wise, while the NL Raman signal is shifted from the laser line, the intensity of each of the fields components, E_0 or E_{Raman} , is locally increased by the neighboring AuNPs, and therefore will affect the scattered signal - the Raman signal. In a bootstrap fashion, we assume that each field component is enhanced by a factor of $1/(1-\alpha_e C_{\text{HF}})$ from the neighboring colloids and concentrating on the scattered field at the shifted Raman frequency,

$$P_{\text{SERS}} = N \cdot g \cdot (\epsilon_0)^2 \cdot (\partial \alpha_m / \partial x)^2 \cdot E_0^2 \cdot E_{\text{Raman}} / (1 - \alpha_e C_{\text{HF}})^3, \quad (3)$$

with $P = Np$. For the laser s-polarization, the coupling constant $C_{\text{HF}} \sim 1.2/\pi a^3 - (8\pi/a^3)K_0(2\pi)$. For metals, the polarizability is $\alpha_e = 4\pi r_0^3$, with r_0 being the colloid radius.

For the 1 mg/mL batch of Fig. 7-8, the average distance between colloids is computed as follows: $(10 \mu\text{L} \text{ per batch}) \times (1 \text{ mg/mL}) \times (1/197 \text{ g/mol}) \times (6.02 \times 10^{23}) \sim 5 \times 10^{15}$ atom of gold. A 45 nm cluster contains $\sim 2.6 \times 10^6$ gold atoms. Thus, the number of clusters is $\sim 10^{10}$ cluster. From [8], a 2 mL and 1 mL batch exhibited similar behavior and strong adhesion, meaning that most, if not all of the AuNPs were attached to the A-C electrodes. The averaged distance between well separated colloids is $\sim (2)^{1/3}/10^5$ per cm, or 100 nm and the coefficient, $\alpha_e C_{\text{HF}} = (1.2/\pi) \cdot 4\pi \cdot (22.5/100)^3 \sim 0.05$. Thus, the denominator is $0.95^3 = 0.85$. Each successive batch decreases the distance between colloids by additional $10 \mu\text{L}$, or about a factor of $\sqrt{10} = 3.16$. The model is valid up to a few titrations before failing (the point where the colloids touch, which also satisfy $1 - \alpha_e C_{\text{HF}} \sim 0$). Beyond that point, the ligand prevents formation of a colloidal array and the signal decreases.

The Zeta potential should give us some indications on the "quality" of the array of colloids. The best results were with the better separated AuNPs (40 nm concentrated and the 45 nm) whereas the lower Zeta potentials, for the as-is 40 nm and 100 nm exhibited a somewhat inferior effect. Overall, both low and high frequencies are effected by the colloids interaction and are depending on the dielectric of the electrolyte.

The enhancement of the G-line over the D-line is a puzzle. From SERS point of view, maximum, single colloid enhancement occurs when the molecule under test is in series to the colloid, namely perpendicular to the colloid surface and in line with the incident field. Otherwise, say under the colloid, the A-C and the colloid are in parallel to each other and SERS is minimized [28]. The points where this condition is met are away from this contact point, between the colloids. As the concentration of AuNPs increases, cooperative effect from neighboring colloids on the polarizable G-line, as opposed to the more symmetric D-line may substantially reduce the I_D/I_G ratio [34].

V. Conclusion

The inclusion of AuNPs colloids, in A-C based supercapacitors just above the electrodes, exhibited not only large amplification of specific capacitance but also a large preference in the ratio of I_D/I_G active-carbon Raman lines. This could suggest a mutual effect of neighboring colloids on both the large specific capacitance and SERS.

References:

1. Maria Hepel, Advances in micro-supercapacitors (MSCs) with high energy density and fast charge-discharge capabilities for flexible bioelectronic devices—A review. *Electrochem. Sci. Adv.* 2022;e2100222. doi.org/10.1002/elsa.202100222
2. L. Miao, Z. Song, D. Zhu, L. Li, L. Gan, M. Liu, Recent advances in carbon-based supercapacitors, *Mater. Adv.* 1 (5) (2020) 945–966.
3. Y. He, X. Zhuang, C. Lei, L. Lei, Y. Hou, Y. Mai, X. Feng, Porous carbon nanosheets: Synthetic strategies and electrochemical energy related applications, *Nano Today* 24 (2019) 103–119
4. Mohammad S. Rahmanifar, Maryam Hemmati, Abolhassan Noori, Maher F. El-Kady, Mir F. Mousavi, Richard B. Kaner, *Materials Today Energy* 12 (2019) 26-36. <https://doi.org/10.1016/j.mtener.2018.12.006>
5. B.K. Kim, S. Sy, A. Yu, J. Zhang, Electrochemical supercapacitors for energy storage and conversion, *Handbook of Clean Energy Systems* (2015) 1–25.
6. Xin Miao, Roberto Rojas-Cessa, Ahmed Mohamed and Haim Grebel, "The Digital Power Networks: Energy Dissemination Through a Micro-Grid", *Proceedings - IEEE 2018 International Congress on Cybermatics*, 230-235. DOI: 10.1109/Cybermatics_2018.2018.00068
7. Roberto Rojas-Cessa, Haim Grebel, Zhengqi Jiang, Camila Fukuda, Henrique Pita, Tazima S. Chowdhury, Ziqian Dong and Yu Wan, "Integration of alternative energy sources into digital micro-grids", *Environmental Progress & Sustainable Energy*, (2018) 37, 155-164. DOI 10.1002/ep.
8. H. Grebel, S. Yu and Y. Zhang, "Active carbon based supercapacitors with Au colloids: the case of placing the colloids in close proximity to the electrode interface", *Nanoscale Adv.*, 2023, 5, 179-190. <https://doi.org/10.1039/D2NA00794K>
9. Brown, John, and Willis Jackson. "The properties of artificial dielectrics at centimetre wavelengths." *Proceedings of the IEE-Part B: Radio and Electronic Engineering* 102.1 (1955): 11-16.
10. R. E. Collin, *Field Theory of Guided Waves*, Wiley-IEEE Press, 2nd edition, 1990.
11. Shih-Chang Wu and H Grebel, "Phase shifts in coplanar waveguides with patterned conductive top covers, *J. Phys. D: Appl. Phys.* 28 437-439 (1995)
12. H. Grebel and P. Chen, "Artificial dielectric polymeric waveguides: metallic embedded films ", *JOSA A*, 8, 615-618 (1991). <https://doi.org/10.1364/JOSAA.8.000615>
13. H. Grebel and P. Chen, "Artificial dielectric polymeric waveguides: semiconductor-embedded films", *Opt. Letts*, 15, 667-669 (1990). <https://doi.org/10.1364/OL.15.000667>
14. Ana Isabel Perez-Jimenez, Danya Lyu, Zhixuan Lu, Guokun Liu and Bin Ren, Surface-enhanced Raman spectroscopy: benefits, trade-offs and future developments, *Chem. Sci.*, 2020, 11, 4563. DOI: 10.1039/d0sc00809e
15. Maier, S. A., *Plasmonics: Fundamentals and Applications*, Springer: New York, 2007.
16. C. Zhang, A. I. Smirnov, D. Hahn, H. Grebel, Surface enhanced Raman scattering of biospecies on anodized aluminum oxide films, *Chemical Physics Letters*, 440(4–6), (2007), 239-243.
17. Paraskevaidis, Kuykendall T, Melli M, Weber-Bargioni A, Schuck PJ, Schwartzberg A, Dhuey S, Cabrini S, Grebel H, "Gain and Raman line-broadening with graphene coated diamond-shape nano-antennas", *Nanoscale*, 30, 2015, 7(37):15321-15331. DOI: 10.1039/c5nr03893f PMID: 26332298.
18. P. Verma, Y. Kuwahara, K. Mori, R. Raja, H. Yamashita, New insights in establishing the structure-property relations of novel plasmonic nanostructures for clean energy applications, *EnergyChem* 4 (2022) 100070

19. Kenichi Ataka, Sven Timo Stripp, Joachim Heberle, "Surface-enhanced infrared absorption spectroscopy (SEIRAS), to probe monolayers of membrane proteins", *Biochimica et Biophysica Acta* 1828 (2013) 2283–2293.
20. Frank Neubrech, Christian Huck, Ksenia Weber, Annemarie Pucci, and Harald Giessen, "Surface-Enhanced Infrared Spectroscopy Using Resonant Nanoantennas", *Chem. Rev.* 2017, 117, 5110–5145. DOI: 10.1021/acs.chemrev.6b00743
21. F. Bonhomme, J. C. Lasse`gues and L. Servant, Raman Spectroelectrochemistry of a Carbon Supercapacitor, *Journal of The Electrochemical Society*, 148(11), E450-E458 (2001)
22. Rafael Vicentini, Leonardo M. Da Silva, Débora V. Franco, Willian G. Nunes, Juliane Fiates, Gustavo Doubek, Luís F.M. Franco, Renato G. Freitas, Cristiano Fantini, Hudson Zanin, Raman probing carbon & aqueous electrolytes interfaces and molecular dynamics simulations towards understanding electrochemical properties under polarization conditions in supercapacitors. *Journal of Energy Chemistry*, 60 (2021) 279–292.
23. John Turkevich, "Colloidal Gold. Part I: HISTORICAL AND PREPARATIVE ASPECTS, MORPHOLOGY AND STRUCTURE", *Gold Bull.*, 1985, 18, 86-91.
24. John Turkevich, "Colloidal Gold. Part II: COLOUR, COAGULATION, ADHESION, ALLOYING AND CATALYTIC PROPERTIES", *Gold Bull.*, 1985, 18, 125-131.
25. Wolfgang Haiss, Nguyen T. K. Thanh, Jenny Aveyard, and David G. Fernig, "Determination of Size and Concentration of Gold Nanoparticles from UV-Vis Spectra", *Anal. Chem.* 2007, 79, 4215-4221.
26. Xiao-Dong Zhang, Di Wu, Xiu Shen, Pei-Xun Liu, Na Yang, Bin Zhao, Hao Zhang, Yuan-Ming Sun, Liang-An Zhang, Fei-Yue Fan "Size-dependent in vivo toxicity of PEG-coated gold nanoparticles", *International Journal of Nanomedicine*, 2011:6 2071–2081. <http://dx.doi.org/10.2147/IJN.S21657>
27. Jörg Stetefeld, Sean A. McKenna, Trushar R. Patel, "Dynamic light scattering: a practical guide and applications in biomedical sciences", *Biophys Rev* (2016) 8:409–427. DOI 10.1007/s12551-016-0218-6
28. Mercado-Lubo, R.; Zhang, Y.; Zhao, L.; Rossi, K.; Wu, X.; Zou, Y.; Castillo, A.; Leonard, J.; Bortell, R.; Greiner, D. L.; Shultz, L. D.; Han, G.; McCormick, B. A. "A *Salmonella* nanoparticle mimic overcomes multidrug resistance in tumours", *Nature Communications* 2016, 12225.
29. H. Grebel, "Surface-enhanced Raman scattering: phenomenological approach", *Journal of the Optical Society of America B* Vol. 21, 429-435 (2004). <https://doi.org/10.1364/JOSAB.21.000429>
30. Duc Le, Martin Kögler, Tian-long Guo, Matthieu Roussey, and Jussi Hiltunen, "Distance-controlled surface-enhanced Raman spectroscopy of nanoparticles", *Optics Letters*, 48, 1454-1457 (2023). <https://doi.org/10.1364/OL.483102>
31. H. Grebel, "Optically Controlled Supercapacitors: Functional Active Carbon Electrodes with Semiconductor Particles", *Materials* 2021, 14(15), 4183; <https://doi.org/10.3390/ma14154183>
31. H. Grebel, "Asymmetric Supercapacitors: Optical and Thermal Effects When Active Carbon Electrodes Are Embedded with Nano-Scale Semiconductor Dots", *C* 2021, 7(1), 7; <https://doi.org/10.3390/c70100072>

32. F. Tuinstra and J. L. Koenig, "Raman Spectrum of Graphite", *J. Chem. Phys.* 53, 1126 (1970); <https://doi.org/10.1063/1.1674108>.
33. Saito, R.; Hofmann, M.; Dresselhaus, G.; Jorio, A.; Dresselhaus, M. S. Raman Spectroscopy of Graphene and Carbon Nanotubes. *Adv. Phys.* 2011, 60, 413–550
34. Golubev, Ye. A.; Rozhkova, N. N.; Kabachkov, E. N.; Shul'ga, Y. M.; Natkaniec-Hołderna, K.; Natkaniec, I.; Antonets, I. V.; Makeev, B. A.; Popova, N. A.; Popova, V. A.; Sheka, E.F., "sp₂ Amorphous carbons in view of multianalytical consideration: normal, expected and new", *J. Non-Cryst. Solids* 2019, 524, 119608.